Concentration and pressure measurements of dense sand and gravel multiphase flows under transient flow conditions in a vertically oriented closed conduit

Assessment of system and sensor performance

van Wijk, J. M.; de Hoog, E.; Talmon, A. M.; van Rhee, C.

DOI
10.1016/j.flowmeasinst.2022.102126

Publication date
2022

Document Version
Final published version

Published in
Flow Measurement and Instrumentation

Citation (APA)
van Wijk, J. M., de Hoog, E., Talmon, A. M., & van Rhee, C. (2022). Concentration and pressure measurements of dense sand and gravel multiphase flows under transient flow conditions in a vertically oriented closed conduit: Assessment of system and sensor performance. *Flow Measurement and Instrumentation*, *84*, Article 102126. https://doi.org/10.1016/j.flowmeasinst.2022.102126

Flow Measurement and Instrumentation 84 (2022) 102126

Contents lists available at ScienceDirect

Flow Measurement and Instrumentation

journal homepage: www.elsevier.com/locate/flowmeasinst

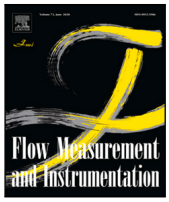

Concentration and pressure measurements of dense sand and gravel multiphase flows under transient flow conditions in a vertically oriented closed conduit — Assessment of system and sensor performance

J.M. van Wijk [a,*], E. de Hoog [b], A.M. Talmon [c], C. van Rhee [d]

[a] Royal IHC; IQIP, The Netherlands[1]
[b] Royal IHC; Delft University of Technology, The Netherlands [2]
[c] Deltares; Delft University of Technology, The Netherlands [3]
[d] Delft University of Technology, The Netherlands [4]

ARTICLE INFO

Keywords:
Dense sediment multiphase flow
Transient flow conditions
Conductivity concentration measurement
Pressure measurement
Density wave attenuation

ABSTRACT

The hydraulic transport of sediments in sediment–water multiphase mixtures is an important process in nature and many industrial applications. The flows are characterized by complex transient phenomena, in which the overall system scale and the particle scale are equally important. Experimental research into dense mixture flows is focused on measurement of flowrates, differential pressures and concentrations of the suspended sediments.

Concentration measurements are especially challenging in the case of coarse particles (beyond millimeter size scale) flowing in dense mixtures, limiting the range of available sensors for accurately measuring the in-situ solids concentrations. For the investigation of transient processes, a quick sensor response is required, which makes concentration measurement based on mixture conductivity an interesting option.

This study is focused on combined concentration and pressure measurements in dense sediment–water mixtures with coarse particles in a vertically oriented closed conduit, using differential pressure sensors over the vertical segments and conductivity probes for measuring the mixture concentration. We experimentally investigated the dispersion process of an initially densely packed batch of sand and gravel by measuring the concentration on different segments of the conduit, resulting in data on mixture wall shear stresses for different sand and gravel mixtures and data of attenuation of concentration gradients in vertical upward and downward flow, in the conduit horizontal top section and in the centrifugal pump.

We describe in the detail the sensor calibration and data processing method, giving a best practice for the use of conductivity concentration sensors in dense coarse particle mixtures, and we suggest a novel method for analysis of density wave amplification and attenuation based on concentration measurements in general, which allows for the detailed analysis of transient multiphase flow phenomena at pipe system component level.

1. Introduction

Hydraulic transport of coarse particle slurries is an important process in nature and many industrial applications. Coarse particle slurries consisting of water as carrier fluid with rocks or sediments as dispersed phase are especially prevalent in the dredging and mining industries. In these applications the pipelines often have many bends, junctions and buffers, introducing a complex transport process with multiple, changing flow-regimes. Horizontal and inclined pipeline configurations exhibit sedimentation of coarse particles and re-suspension by erosion, giving rise to a wide variety of transport regimes ranging from stationary deposits to pseudo-homogeneous flows, depending on particle properties and flow velocities [1–7].

Design of hydraulic transport systems is mostly limited to steady state analyses, in which the mixture velocity and solids concentration are assumed constant in time. Flow regimes are accounted for by

* Corresponding author.
E-mail addresses: Jortvanwijk@iqip.com (J.M. van Wijk), e.dehoog@royalihc.com (E. de Hoog), a.m.talmon@tudelft.nl (A.M. Talmon), c.vanrhee@tudelft.nl (C. van Rhee).

[1] www.royalihc.com; www.iqip.com.
[2] www.royalihc.com; www.tudelft.nl.
[3] www.deltares.nl; www.tudelft.nl.
[4] www.tudelft.nl.

https://doi.org/10.1016/j.flowmeasinst.2022.102126
Received 8 October 2021; Received in revised form 13 December 2021; Accepted 11 January 2022
Available online 22 January 2022

Nomenclature

Parameters

α	Water conductivity temperature correction coefficient [K^{-1}]
a	Empirical parameter in settling velocity equation [–]
b	Empirical parameter in settling velocity equation [–]
c_v	Volumetric concentration [–]
c_{vd}	Delivered volumetric concentration [–]
$c_{v,eq}$	Volumetric concentration of perfectly homogeneous mixture [–]
$c_{v,p}$	Peak volumetric concentration [–]
$c_{v,t}$	Trough volumetric concentration [–]
$c_{v,r}$	Volumetric concentration in riser [–]
$c_{v,rp}$	Volumetric concentration in return pipe [–]
$c_{v,r}$	Volumetric concentration in riser [–]
C_D	Drag coefficient [–]
d	Particle diameter [m]
d_m	Mean particle diameter [m]
d_{50}	Median particle diameter [m]
D	Pipe diameter [m]
δ	Logarithmic decrement [–]
ϵ_z	Axial dispersion coefficient [m^2/s]
g	Gravitational acceleration [m/s^2]
h_i	Initial batch height [m]
k_f	Fluid conductivity [S/m]
k_m	Mixture conductivity [S/m]
λ	Darcy–Weisbach friction factor [–]
L_b	Batch length [m]
L_c	Conduit length [m]
μ	Water viscosity [Pa s]
n	Hindered settling exponent [–]
N	Pump speed [rpm]
p	Pressure [Pa]
Δp	Differential pressure [Pa]
Δp_r	Differential pressure in the riser [Pa]
Δp_{rp}	Differential pressure in the return pipe [Pa]
Pe	Peclet number [–]
ρ_f	Water density [kg/m^3]
ρ_s	Solid's density [kg/m^3]
R	Ratio of riser and return pipe concentrations [–]
Re	Reynolds number [–]
Re_p	Particle Reynolds number [–]
St	Stokes number [–]
t	Time [s]
t_c	Timescale of flow through conduit [s]
t_e	Timescale of largest turbulent eddy [s]
t_p	Particle response time [s]
τ_f	Fluid wall shear stress [Pa]
τ_m	Mixture wall shear stress [Pa]
v_{hs}	Hindered settling velocity [m/s]
v_m	Mixture velocity [m/s]
v_{ts}	Terminal settling velocity [m/s]
v_s	Solid's transport velocity [m/s]
ξ	Empirical exponent in Archie equation [–]
ζ	Empirical exponent in Van Wijk and Blok's equation [–]
Δz_r	Spacing between differential pressure sensor connections in riser [m]
Δz_{rp}	Spacing between differential pressure sensor connections in return pipe [m]

Abbreviations

CCM	Conductivity Concentration Meter

different friction loss models and the application of slip ratio models, which give the material distribution in the pipeline (modeled as a bed layer and homogeneous mixture on top). Transient effects are mostly neglected, under the assumption that transients will be smoothed out rapidly. This however has proven to be insufficient for explaining a number of reported cases in which transient effects dominated the operation of the transport system.

In vertical configurations there is less variation in flow regimes, but especially large or heavy particles can give rise to the occurrence of density waves, local particle agglomeration or even plug formation [8]. Successive experimental work on vertical transport systems as described in Mueller et al. [9] showed a glimpse of unstable transient effects that were encountered during the large scale vertical transport tests in the Blue Mining project. The Blue Mining test setup consisted of a 130 m riser and return pipe with $D = 145$ mm, mounted in an abandoned mine shaft, with another 63 m of horizontal pipeline. In these experiments we have witnessed the steady agglomeration of initially homogeneously dispersed sediments (sand, gravel) into a highly concentrated batch, inducing heavy fluctuations of the mixture velocity as well. The system was highly unstable. Another case of highly unstable hydraulic transport occurred during the construction of the Prins Clausplein in the Netherlands, for which a 10 km pipeline was used. This case, the Blue Mining experiments and other cases are discussed in more detail in De Hoog et al. [10], who report on several cases of unstable transients (growing density waves), which adversely affect flow assurance.

Stability of the transport process clearly is not a given and design for steady state conditions only, is not sufficient. Transient modeling of transport systems is indispensable for flow assurance in long, complex transport systems handling coarse particle slurries. However, literature on (unstable) transients in hydraulic transport systems is extremely scarce and modeling of these systems is still in an early phase. When incorporating flow assurance in hydraulic transport system design, it is essential to identify and understand the underlying physics of these transient phenomena.

Accurate measurement of the mixture density or concentration (volume fraction of solids) is indispensible for understanding sediment–water transport. Mixture concentrations >10% by volume are no exception and measurement of transient phenomena requires quick response times ($\mathcal{O}(10^{-1}$ s) timescale). Different concentration measurement techniques exist [11] and have been reviewed to support the choice of sensors in the current work. Density measurements by weighing of a pipe segment or U-loop differential pressure measurements provide spatial averaged values, not local concentrations. Gamma densitometers are well known for their industrial application in dredging and mining, however their poor response time (due to time averaging) and the radio active source makes them not practical for laboratory use focused on small timescale phenomena. Electrical resistance measurement and conductivity measurement have been successfully applied in multiphase flow measurement, either to give cross-section averaged concentrations or complete concentration distributions over the cross-section. Resistance or conductivity measurements are known for their quick response time and flexible integration in different test setups, which motivated the choice for implementing conductivity concentration meters in this work. In [12] the development of a concentration measurement sensor is described which was specifically designed for sediment–water mixtures with coarse particles. This sensor uses four

pairs of conductivity probes, aligned opposite of each other spanning the diameter of the sensor pipe. In the current work we use these conductivity probes.

In this article we present 13 experiments being conducted with four types of coarse sand and gravel. The main idea is to follow a well-defined batch of solids when it flows through the conduit and gets dispersed when it passes through a riser, horizontal top section, return pipe and a centrifugal pump. By measuring the solids concentration on each corner of the conduit with the conductivity concentration sensors described in Van Wijk and Blok [12], the differential pressures over the riser and return pipe and the mixture velocity we are able to study the development of the peak concentration of the batch for each component in the system.

In this way it is possible to study the CCM performance for a wide range of mixture properties, in terms of solids concentration and sediment size. This research provides insight in the possibilities and limitations of conductivity concentration sensors and we describe the best practice for their application. Furthermore, we provide a novel method for analysis of density wave growth or attenuation based on concentration measurements, which is generally applicable. The paper provides a comprehensive discussion of the test setup, sensor calibration, measurement and data processing methods and the flow phenomena observed.

2. Materials and methods

2.1. The closed conduit test setup

The hydraulic conduit and its main components are shown in Fig. 1. The flow is generated by a centrifugal pump (Linatex D4 driven by an 11 kW electromotor with frequency drive) and runs through a riser section, a return pipe and it can be bypassed to a hopper for emptying the system. The setup is equipped with an electromagnetic flowmeter in the return pipe (Krohne Optiflux 4000 with an inner diameter of $D = 100$ mm) and a PT100 temperature sensor to measure the water temperature. The conduit has a volume of 0.0979 m^3.

Both the riser and return pipe are equipped with PTX 2100 differential pressure sensors with a range of 0–200 kPa. Both sensors have an accuracy of ±0.3% (deviation from linear relation between extrema of the scale). The sensors are equipped with synthetic foam at the water intake to prevent solids from entering the sensor. Differential pressures are defined as $\Delta p_r = p_1 - p_2$ for the riser and $\Delta p_{rp} = p_3 - p_4$ for the return pipe. The setup also has an absolute pressure sensor and camera. The absolute pressure sensor was not used in the current experiments. The camera was used to film the batch transport and to be able to study the differences in flow processes of sand and gravel.

In order to measure the concentration development in the flowloop, the riser and return pipe are equipped with conductivity concentration meters (CCM). One CCM device consists of a pipe segment with internal diameter $D = 99.4$ mm in which four pairs of platinum electrodes are mounted. Each electrode is aligned exactly opposite to its matching electrode to form a pair. Each electrode is mounted flush in the wall. A pair measures the conductivity of the fluid, the four pairs are averaged to a single conductivity signal (in volts) by the software enclosed in the purpose-built hardware. See Van Wijk and Blok [12] for more details on their design. The distance between the CCM sensors in the riser section measures 2970 mm, the distance between the pressure transducers measures 2540 mm. In the return pipe, the CCM sensors are 3320 mm apart and the pressure transducers are 2780 mm apart. Both upper bends have a radius of 170 mm, the horizontal pipe section at the top measures 730 mm. The distance between the CCM's should be as large as possible in order to maximize the measurement result when comparing the results in upward and downward transport, but consequently the distance from the CCM's to the bends and pump outlet are relatively small. All sensors are connected to a Dataq Instrument data-acquisition system sampling with 100 Hz per channel.

2.2. Experiment program

The experiments are conducted with two types of sand and two types of gravel with a subrounded to subangular shape and estimated grain density of 2650 kg/m^3. Fig. 2 shows the particle size distributions of Sand 1, Sand 2 and Gravel 1 (of Gravel 2, only the under and oversizes are specified). Sands 1 and 2 have a maximum over- and undersize of 5% and gravels 1 and 2 have a maximum under- and oversize of 10%. We determined the packed bed concentration of the sediments based on the inserted dry mass of sediment and the water displacement in the test setup. The sediments were loosely poured and not compacted to ease the fluidization of the batch at the start of an experiment. For sand 1 this resulted in $c_v = 0.56$ for sand and $c_v = 0.59$ for gravels 1 and 2 . Next to the packed bed concentration, also the homogenized concentration $c_{v,eq}$ is calculated, which is defined as the ratio of sediment volume over the conduit volume. Due to gravity, the concentration in the riser will be larger than the concentration in the return pipe. The homogenized concentration can be considered as the average of the two (assuming no significant amounts of material remain in the horizontal sections of the conduit).

In the experiments we vary the sediment type (two sizes of sands, two sizes of gravel), the initial batch height, which determines the equilibrium concentration in an experiment and the average mixture velocity in the conduit, resulting in a total of 13 experiments.

An experiment starts with inserting a batch of solids in the riser section onto the closed gate valve. Then the pump is started so that pressure can build up. When the pump has reached its preset speed, the valve is opened and water penetrates the plug quickly. Initially the plug has some wall resistance due to gravity pressing the batch of solids to the valve, which induces radial stresses and thus wall friction. Upon opening the valve, this friction gets lower due to the fluidization process and the plug starts to accelerate. On its way through the riser, the return pipe, the bends and the pump the plug gradually disperses. An experiment ends with a more or less homogeneous mixture that fills the conduit.

The particle properties are summarized in Table 1.

3. Data analysis method

3.1. Basic relation between conductivity and volume fraction of solids

The CCM's are conductivity sensors. The relation between electrical conductivity and c_v can be modeled with the Effective Medium Theory [13]. The CCM output is related to conductivity by calibration of the fluid phase. The conductivity of the fluid phase is denoted k_f, the conductivity of the mixture is denoted k_m. The fluid conductivity k_f and mixture conductivity k_m are related to the volume fraction of solids or concentration c_v.

The output of a CCM sensor has two extrema. When the sensor is filled with air (which has zero conductivity), the situation is comparable to the measurement section entirely filled with a non-conductive solid cylinder. In this case, the CCM output signal is given a numeric value of 1 in the software. When the measurement section is entirely filled with water, conductivity is maximal and the CCM output signal is given a value of 0. In this way, the CCM output is $(1-k_m/k_f)$ determined at a reference temperature of $T = 17\,°C$ (tapwater temperature as measured during setting up the experiment).

The conductivity of water is strongly dependent on the water temperature [14]. We measured the output of the four CCM's filled with tap water at temperatures between 16 °C and 28 °C from which the linear relation $\left(1 - k_m/k_f\right)|_{T_{ref}} - \left(1 - k_m/k_f\right)|_T = -\alpha \cdot \left(T - T_{ref}\right)$ was found with $\alpha = 0.0238$.

In this work we have a non-conductive solid phase. Banisi et al. [15] suggests the models of Maxwell ($\frac{k_m}{k_f} = \frac{2-2\cdot c_v}{2+c_v}$ for monodisperse mixtures or narrowly graded mixtures) and Bruggeman ($\frac{k_m}{k_f} = \left(1 - c_v\right)^{3/2}$ for

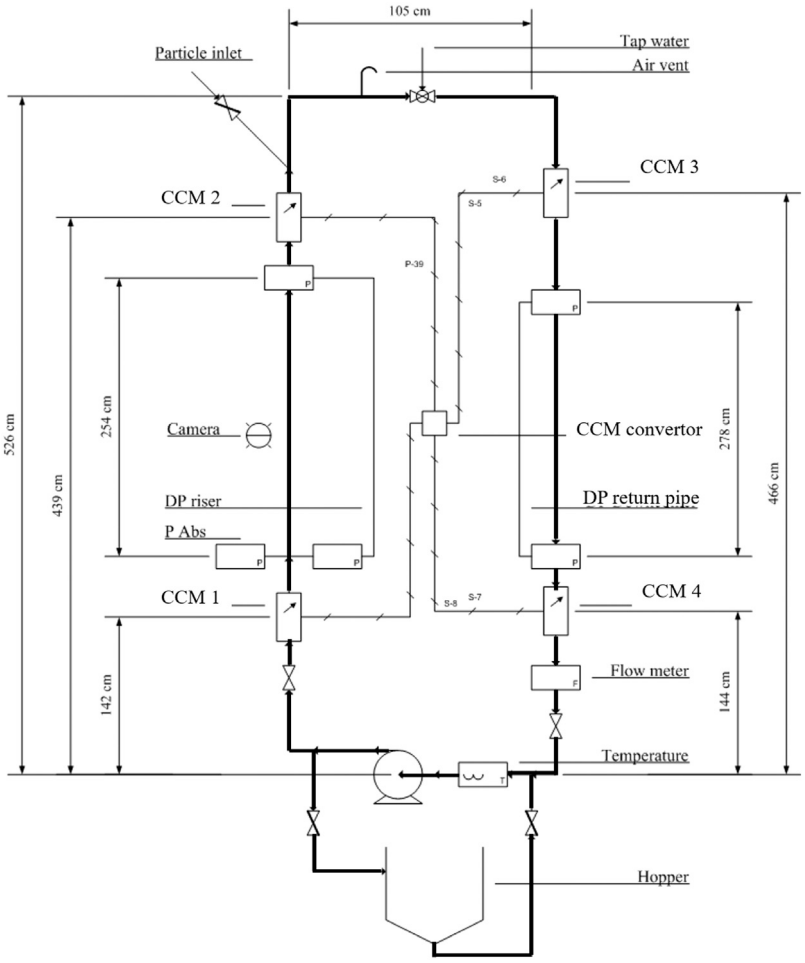

Fig. 1. Schematic representation of the test setup and its main components.

Table 1
Experiments and their specifications.

Exp. no.	d [mm]	d_{50} [mm]	d_m [mm]	$L_b = h_i$ [m]	$c_{v,eq}$ [–]	v_m (st. state) [m/s]
1	0.2–0.5	0.39	0.42	1.0	0.044	2.0
2	0.2–0.5	0.39	0.42	1.0	0.044	2.96
3	0.2–0.5	0.39	0.42	1.0	0.044	3.95
4	0.8–1.25	1.05	1.10	0.40	0.018	2.08
5	0.8–1.25	1.05	1.10	1.0	0.044	1.99
6	0.8–1.25	1.05	1.10	2.0	0.089	1.89
7	0.8–1.25	1.05	1.10	1.0	0.044	3.02
8	5.0–8.0	6.34	6.60	1.0	0.047	1.94
9	5.0–8.0	6.34	6.60	1.5	0.070	1.85
10	5.0–8.0	6.34	6.60	2.0	0.094	1.78
11	5.0–8.0	6.34	6.60	1.0	0.047	2.85
12	8.0–16.0	12.0	6.60	1.0	0.047	1.85
13	8.0–16.0	12.0	12.0	1.0	0.047	2.81

wide particle size distributions) for conductivity concentration meters. Although the theoretical grounds of the Maxwell model set an upper limit to the volume fraction of solids of $c_v = 0.2$, in practice it proves to perform well up to $c_v = 0.5$, especially with fine particles, and it is therefore commonly used [15–18]. The CCM's principle is similar to the ERT systems investigated in Xu et al. [19] and Faraj and Wang [20], although the ERT's are aimed at 2D cross-section visualization of concentrations and have more electrodes than our CCM's. These studies focused on ERT performance with slurry flows having $0.05 \leq c_v \leq 0.15$ and particles with 355 μm $\leq d_m \leq$ 560 μm. Faraj and Wang [20] reports a random error of 19% for concentration measurements ($c_v = 0.1$) with the ERT in combination with the Maxwell relation. A model similar to Bruggeman's is the Archie equation [21], who left the exponent open as an empirical parameter to acknowledge the fact that calibration is needed depending on the solids at hand, $\frac{k_m}{k_f} = \left(1 - c_v\right)^{\xi}$.

The calibrations of the CCM's used in this work have been investigated in detail, see Van Wijk and Blok [12]. Especially for the larger particles (diameters in the order of millimeters, e.g. the gravels used in this experiment), the traditional models do not perform well with the CCM's and therefore an alternative calibration was proposed:

$$\frac{k_m}{k_f} = 1 - c_v^{\xi} \tag{1}$$

In this work, we will determine the exponent ζ per experiment in order to have the most accurate measurement of c_v.

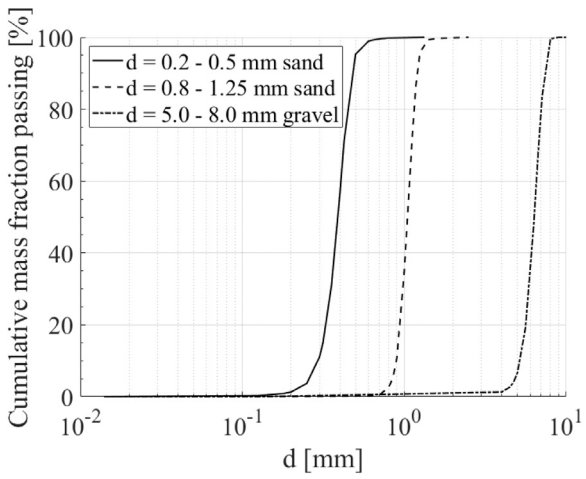

Fig. 2. Particle size distribution of the sediments used in the experiments.

3.2. Data processing method

We need to apply a series of processing steps to convert the raw CCM data to the volume fraction of solids c_v. The initial temperature distribution in the test setup is unknown, and only after a few cycles the temperature can be assumed homogeneous throughout the system. For future experiments it is recommended to have the water well-mixed before starting an actual experiment. For the current experiments we need a correction procedure according to the next steps:

1. Align the zero's of CCM2 and CCM3.
2. Align the equilibrium concentrations of CCM1 with CCM2 and of CCM4 with CCM3.
3. Calibrate Eq. (1) with the equilibrium concentration $c_{v,eq} = 0.5 \cdot (c_{v,r} + c_{v,rp})$.

A more detailed explanation of the above steps follows next.

After filling the conduit with tap water at $T \approx 17$ °C, the water was used for multiple experiments. During pumping heat is added to the water and temperature rises. When at rest, warm water moves upward to CCM's 2 and 3, which results in temperature gradients when the system was left unused for a while. The valve just below CCM1 further complicates the temperature distribution. Due to these different processes the initial temperature distribution during a new test was unknown and a sequence of corrections was applied. For future work it is highly advised to change water every new test.

The CCM's have been calibrated prior to the experimental campaign, so it is safe to assume they have no offset with respect to each other, and any offset is due to gradients in temperature and conductive soluble material. CCM's 2 and 3 are at equal height in the setup and should therefore have equal zero reading prior to testing. Since the CCM's are filled with water, both are shifted toward zero. This step can be seen as an implicit temperature correction to the CCM data.

The next step in correcting the raw CCM data, is looking at the equilibrium concentrations in the riser ($c_{v,r,eq}$) and return pipe ($c_{v,rp,eq}$). $c_{v,r,eq}$ as measured by CCM2 near the end of an experiment (time averaged over the final 25% of the measured timespan) should equal $c_{v,r,eq}$ as measured by CCM1, and CCM1 is corrected for this. A similar approach is used for the correction of CCM4, which should give an $c_{v,rp,eq}$ reading equal to CCM3. This step can be seen as a second implicit temperature correction of CCM's 1 and 4.

One can argue whether the direct temperature correction using [14] should be used. This has been tried as well, but with unsatisfactory results. Due to the valve below CCM 1 and the temperature gradient present in the system prior to an experiment, the temperature reading at the bottom of the conduit is not representative for any pockets of water with different temperatures that need to be mixed during the first few round of the sediment batch through the conduit. In some experiments, a step in temperature of as much as 1–2 °C was observed in the first seconds, having significant influence on the overall temperature correction. The above procedure gave better results overall. Again, this could have been avoided by using fresh water for every new experiment. It needs to be noted here as well that in the transient analysis, we will use a relative measure of the batch dispersion, which is not depending on the absolute values of the CCM reading. In this way the inaccuracy introduced by above steps does not propagate in the actual assessment of batch dispersion.

The final correction step is the conversion of the conductivity readings of the CCM's to the actual concentration. For this Eq. (1) is used, and the parameter ζ has been determined for each experiment in order to have $c_v \approx 0.5 \cdot (c_{v,r,eq} + c_{v,rp,eq})$, with c_v known from the total mass of solids loading in the system. An overview of the values of ζ is given in Fig. 4. We verified the calibration by comparing the actual packed bed concentration with the reading of CCM 1 prior to testing, which is also shown in Fig. 4. At low concentrations the CCM's are calibrated to have the smallest error possible (near zero), while the data at the packed bed concentration fall within a ±25% bandwidth except for one outlier. The bandwidth 0–25% is considered representative for typical CCM measurements, with an increasing error with increasing concentrations. The error is of comparable order as the error reported in Faraj and Wang [20].

A moving average filter is applied to reduce the high frequency noise that is present on the different signals, due to different reasons. Especially the gravel experiments show noise: the velocity readings show noise due to collisions between gravel and the electromagnetic flow meter inner tube (causing small elastic deformations and inductive noise on the coils), the pressure readings show noise due to vibrations and grounding and the CCM's show noise due to grounding as well (an issue that has been investigated in successive research and which was resolved by improved grounding). With a sampling frequency of 100 Hz we used a window size of 20 on the measurement data so to have averaging on the scale of 0.05 s.

All steps are illustrated in Fig. 3, showing the data of Experiment 5 from Table 1. As can be observed, some signals suffer from negative values which remain after correction. The most probable explanation for this, is the presence of conductive material (minerals from the sediments, abraded steel from the pump). When mixed, this material could artificially increase the mixture conductivity and thereby reduce the measured solids concentration, which introduces an error in the absolute values of c_v but which does not influence the actual shape of the signals, which makes studying the transport processes still possible.

The total uncertainty in the measurement of c_v is determined by the uncertainties introduced by the temperature distribution in the water, especially at the onset of the experiment, the uncertainty introduced by the presence of contaminants and the uncertainty introduced by the actual calibration model used to convert conductivity into volume fraction of solids.

3.3. Data analysis

The processed data is analyzed to find:

1. Solids transport (concentration, velocity) with fully dispersed sediment batch.
2. Pressure drop in the riser and return pipe with fully dispersed sediment batch.
3. Particle inertia and the relative dominance of advection and turbulent diffusion (radial mixing).
4. Attenuation of concentration gradients on the scale of the conduit.

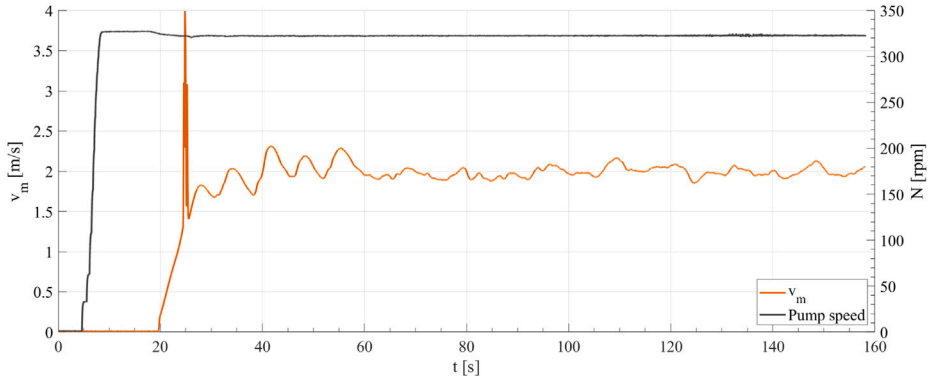

(a) Mixture velocity and pump speed.

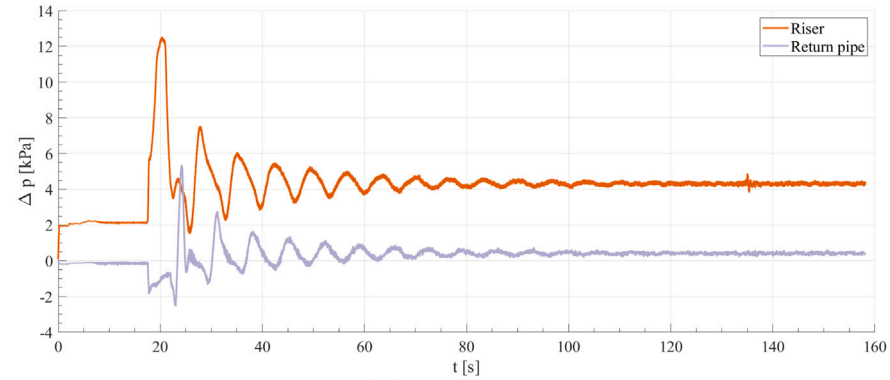

(b) Δp measurements.

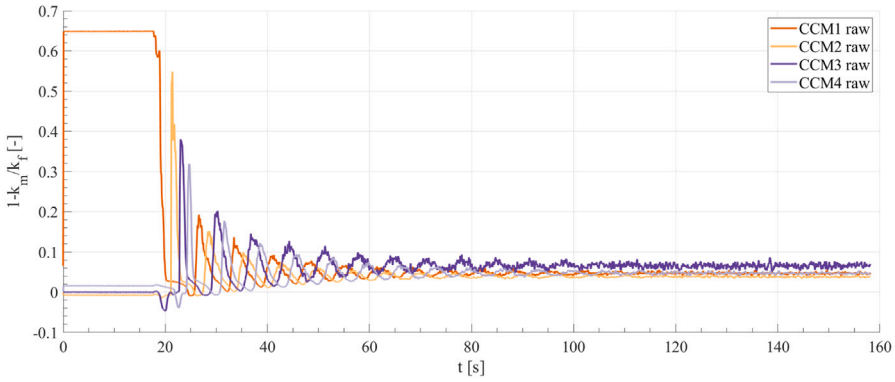

(c) Raw CCM data.

Fig. 3. Example of data and processing steps for Experiment 5. Batch transport and dispersion of $d_m = 1.05$ mm sand.

Details of the analyses are given in the next sections. We will differentiate two cases. First we discuss the fully dispersed batch cases, in which the concentrations in riser and return pipe have reached more or less constant values (which was always the case near the end of the experiments). Second, we discuss the transport of the sediment batch before being fully dispersed, which will be called the transient condition.

3.3.1. *Fully dispersed batch*

After a number of cycles through the conduit, the batch of solids is fully dispersed and the riser and return pipe concentrations reach a more or less steady value. This state of the system will be further investigated in this section The general flow condition is characterized by the Reynolds number $Re = \rho_f \cdot v_m \cdot D/\mu$, with $\mu \approx 1.08 \cdot 10^{-3}$ Pa s for fresh water at $T = 17\,^{\circ}$C and v_m measured by the electromagnetic flowmeter. The quasi steady-state analysis will be conducted with the mean values of measured velocities, pressures and concentrations. To this end, the mean of the last 25% of each data set will be taken.

For the concentrations as measured with the CCM's, the steady state concentrations in the riser and return pipe are then defined as the mean of the two CCM's in the riser and return pipe respectively, of which the time average over the final 25% of the measurement data is taken. For the riser:

$$\overline{c_{v,r}} = 0.5 \cdot \left(\int_{t1}^{t2} c_{v,ccm1}\, dt + \int_{t1}^{t2} c_{v,ccm2}\, dt \right) \tag{2}$$

with $t1 = 3/4 \cdot t_{measurement}$ and $t2 = t_{measurement}$. Equally for the return pipe:

$$\overline{c_{v,rp}} = 0.5 \cdot \left(\int_{t1}^{t2} c_{v,ccm3}\, dt + \int_{t1}^{t2} c_{v,ccm4}\, dt \right) \tag{3}$$

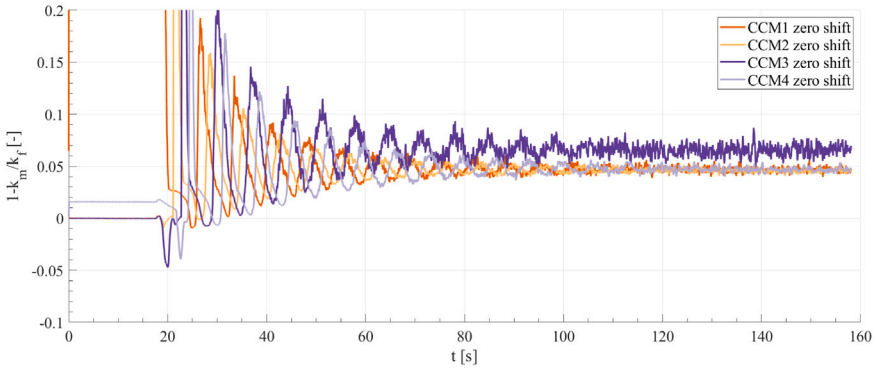

(d) Zero alignment CCM 2 and 3 (step 1).

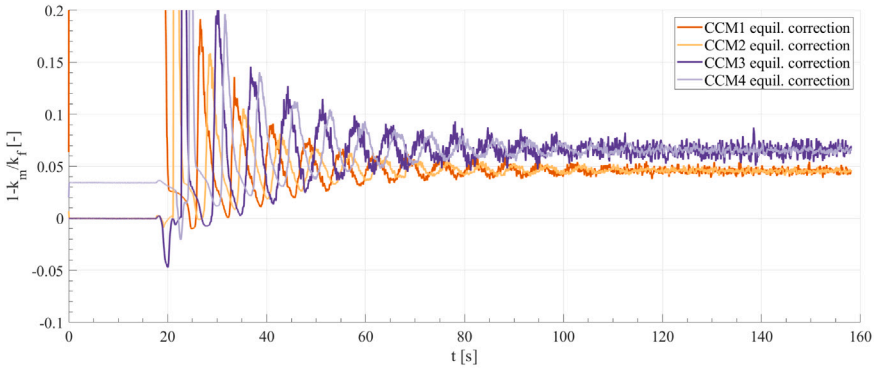

(e) Equilibrium correction CCM1 and 4 (step 2).

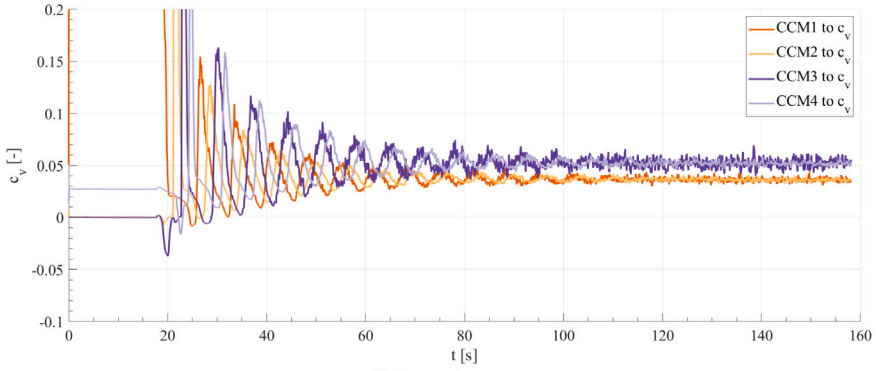

(f) Conversion to c_v.

Fig. 3. (*continued*).

A similar averaging approach is followed for the differential pressure measurements:

$$\overline{\Delta p} = \int_{t1}^{t2} \Delta p \, dt \tag{4}$$

Following the work of Clift and Manning-Clift [22], the differential pressure measurements at the stable equilibrium conditions in the riser and return pipe can also be used to estimate for the delivered concentration c_{vd} and the concentrations in the riser and return pipe, which provides an additional measurement of the concentrations. Let $c_{v,r}$ be the concentration in the riser and let $c_{v,rp}$ be the concentration in the return pipe. The sum of both can expressed in terms of the differential pressure measurements over distance Δz:

$$c_{v,r} + c_{v,rp} = \left(\frac{\overline{\Delta p_r}}{\Delta z_r \cdot g} - \frac{\overline{\Delta p_{rp}}}{\Delta z_{rp} \cdot g} \right) \cdot \frac{1}{\rho_s - \rho_f} \tag{5}$$

The sum of $c_{v,r}$ and $c_{v,rp}$ can also be expressed in terms of the delivered concentration c_{vd}, mixture velocity v_m and the hindered settling velocity v_{hs} at $c_v = c_{vd}$ with hindered settling exponent n:

$$c_{v,r} + c_{v,rp} = 2 \cdot c_{vd} \cdot \left(1 + \frac{v_{hs}(c_{vd})^2}{v_m^2} \cdot \left[1 - \frac{n \cdot c_{vd}}{1 - c_{vd}} \right] \right) \tag{6}$$

Eqs. (5) and (6) can be solved to find c_{vd}. The riser concentration $c_{v,r}$ now can be found from iteratively solving:

$$c_{vd} \cdot v_m = c_{v,r} \cdot \left(v_m - v_{hs}(c_{v,r}) \right) \tag{7}$$

and the return pipe concentration $c_{v,rp}$ follows from iteratively solving:

$$c_{vd} \cdot v_m = c_{v,rp} \cdot \left(v_m + v_{hs}(c_{v,rp}) \right) \tag{8}$$

The hindered settling velocity follows from the terminal settling velocity of a single particle v_{ts}, corrected for the presence of surrounding particles expressed in c_v. The influence of surrounding particles on the settling velocity of a single particle has been extensively investigated in the past decades, with the model of Richardson and Zaki [23] still

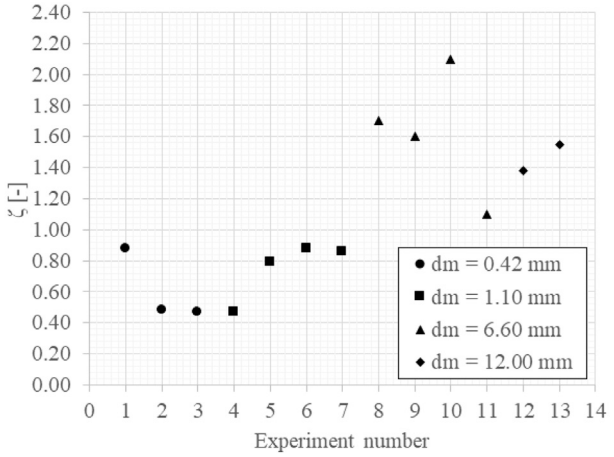

(a) Calibration parameter ζ.

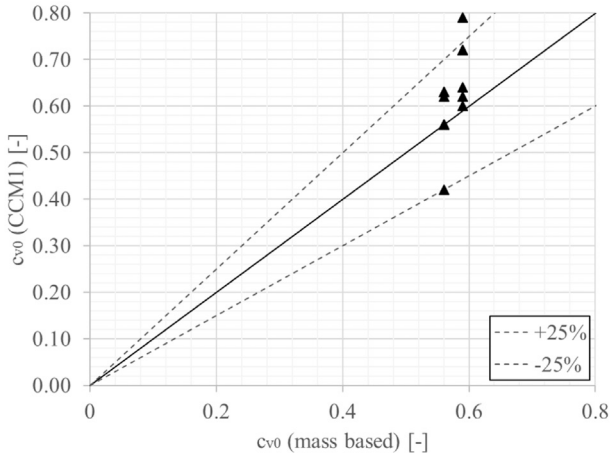

(b) $c_{v,0}$ CCM1 measurement compared with the packed bed concentration based on inserted mass of sediment.

Fig. 4. Calibration parameter ζ used in Eq. (1).

being relevant. An increasing volume fraction of solids will result in a decrease in settling velocity:

$$v_{hs} = v_{ts} \cdot \left(1 - c_v\right)^n \tag{9}$$

While Clift and Manning-Clift [22] use the hindered settling velocity of Eq. (9). According to Richardson and Zaki [23], this equation holds for settling in still water, while during fluidization an additional multiplication factor $10^{-d/D}$ should be included. Especially for particles with large diameters d, this has a significant influence on the slip velocity, with Eq. (9) overestimating the actual hindered settling velocity up to 26% for the $d_m = 12$ mm gravel. In our analysis we have included the factor. The hindered settling exponent n can be approximated as a function of the particle Reynolds number $Re_p = \rho_f \cdot v_{ts} \cdot d/\mu$ as $n = \left(4.7 + 0.41 \cdot Re_p^{0.75}\right) / \left(1 + 0.175 \cdot Re_p^{0.75}\right)$ [24].

A single particle settling in an undisturbed fluid will settle with its terminal settling velocity v_{ts}, which results from a balance between gravity, buoyancy and drag forces. For sediments, the empirical model of Ferguson and Church [25] is an accurate approximation:

$$v_{ts} = \frac{\rho_s - \rho_f}{\rho_f} \cdot g \cdot d^2 \cdot \left(a \cdot \mu/\rho_f + \left[b \cdot 0.75 \cdot \frac{\rho_s - \rho_f}{\rho_f} \cdot g \cdot d^3 \right]^{0.5} \right)^{-1} \tag{10}$$

With $a = 18$ and $b = 1.1$ for natural, sieved sands.

In an upward flow, the resulting solids velocity is:

$$v_s = v_m - v_{hs} \tag{11}$$

In downward flow the sign of the hindered settling velocity is reversed. Since continuity demands $c_v \cdot v_s = constant$ throughout the conduit, we can estimate the ratio of the riser and return pipe concentrations R as follows:

$$R = \frac{c_{v,r}}{c_{v,rp}} = \frac{v_m - v_{ts} \cdot \left(1 - c_v\right)^n}{v_m + v_{ts} \cdot \left(1 - c_v\right)^n} \tag{12}$$

During transport, the pipelines exert friction on the flowing mixture. The wall shear stress τ_m at quasi steady-state conditions can be found from:

$$\tau_m = \frac{D}{8} \cdot \left(\frac{\overline{\Delta p_r}}{\Delta z_r} - \frac{\overline{\Delta p_{rp}}}{\Delta z_{rp}} - 2 \cdot g \cdot (\rho_s - \rho_f) \cdot c_{vd} \cdot \frac{v_{hs}(c_{vd})}{v_m} \right) \tag{13}$$

3.3.2. Transient conditions

The processes in the conduit show three important timescales. The first is the timescale of the entire conduit, which is $t_c = L_c/v_m$. With the conduit length $L_c = 12.6$ m and $1 < v_m \approx 3$ m/s as the range of mixture velocities. The second important timescale is related to the largest turbulent eddies present in the conduit: $t_e = D/v_m$, with $D = 0.0994$ m. The third timescale is related to particle inertia, which is a result of particle density and size. In Van Wijk et al. [26] this timescale was based on the terminal settling velocity of the particles and the particle diameter. However, a better approach would be to base the particle response time on the acceleration of the particle from rest to $0.63 \cdot v_{ts}$ as was done in Van Wijk et al. [27]. Solving the equation of motion of a submerged sphere under influence of gravity, buoyancy and drag, with the drag coefficient of Brown and Lawler $C_D = 24/Re_p \cdot \left(1 + 0.15 \cdot Re_p^{0.681}\right) + 0.407/\left(1 + 8710/Re_p\right)$ as shown in the review article of Cheng [28] gives the particle timescales t_p.

From these timescales we define the Stokes number $St = t_p/t_e$, with $St \ll 1$ an indication of the particles being subjected to turbulent dispersion, and $St \gg 1$ and indication of the particles being relatively insensitive to turbulent dispersion.

The remaining question is the relative dominance of advection processes and turbulent dispersion processes, which can be analyzed with the particle Peclet number, with L_b the batch length and ϵ_z the axial dispersion coefficient as a measure of turbulent dispersion of the sediments:

$$Pe = \frac{v_{ts} \cdot L_b}{\epsilon_z} \tag{14}$$

As shown in Van Wijk et al. [26] the upper limit of ϵ_z is given by Taylor dispersion [29], $\epsilon_z = 10.1 \cdot D/2 \cdot \sqrt{\tau_f/\rho_f}$, with $\tau_f = \lambda/8 \cdot \rho_f \cdot v_f^2$ the wall shear stress of water and λ the Darcy–Weisbach friction factor. For increasing Stokes numbers it was found that ϵ_z goes to zero. For L_b the lower limit would be the initial batch length. This combination of L_b and ϵ_z gives a conservative estimate of Pe.

After the time scale and process characteristics analysis, we look at the actual attenuation of the concentration gradients in the riser, return pipe and centrifugal pump. The attenuation is the result of two processes. First, a steep concentration gradient and associated diluted tail of the batch develops as a result of the advection process, which is dominated by the nonlinear relation between the solids concentration and propagation velocity. Second, there is the process of turbulent mixing of the sediments. Both processes happen simultaneously, with for many of the experiments advection being (slightly) dominant over dispersion, but the latter not being negligible. Van Wijk et al. [26] took into account a correction for the advection process to isolate the turbulent diffusion process, and was able to provide a relative measure of axial dispersion (relative to Taylor dispersion) for sediment transport over 8.655 m transport length through a riser. In the current experiments, the batch of sediments is large compared to the riser and return pipe lengths, which makes it very difficult to separate the different processes without introducing additional uncertainties. It can be the case that the tail of a batch is still in the riser, the main part of the batch is in the horizontal line at the top while the head of the

Table 2
Calculation of flow conditions per experiment.

Exp. no.	v_{ts} [m/s]	Re [–]	Re_p [–]	t_p [s]	t_e [s]	St [–]	ϵ_z [m^2/s]	Pe [–]
1	0.053	$1.81 \cdot 10^5$	20.2	0.0047	0.050	0.095	0.071	0.75
2	0.053	$2.76 \cdot 10^5$	20.2	0.0047	0.034	0.14	0.11	0.51
3	0.053	$3.57 \cdot 10^5$	20.2	0.0047	0.025	0.19	0.14	0.38
4	0.13	$1.88 \cdot 10^5$	130	0.0013	0.048	0.27	0.074	0.71
5	0.13	$1.80 \cdot 10^5$	130	0.0013	0.050	0.26	0.070	1.85
6	0.13	$1.71 \cdot 10^5$	130	0.0013	0.053	0.25	0.067	3.89
7	0.13	$2.73 \cdot 10^5$	130	0.0013	0.033	0.40	0.11	1.22
8	0.37	$1.75 \cdot 10^5$	2220	0.058	0.051	1.13	0.069	5.39
9	0.37	$1.67 \cdot 10^5$	2220	0.058	0.054	1.08	0.065	8.49
10	0.37	$1.61 \cdot 10^5$	2220	0.058	0.056	1.04	0.063	11.76
11	0.37	$2.58 \cdot 10^5$	2220	0.058	0.035	1.66	0.10	3.67
12	0.58	$1.67 \cdot 10^5$	6327	0.084	0.054	1.56	0.065	8.87
13	0.58	$2.54 \cdot 10^5$	6327	0.084	0.035	2.37	0.099	5.84

batch is already accelerating downward through the return pipe. For these situations one cannot separate advection from axial dispersion, hence in the current analysis the attenuation of the peak concentration due to the different processes occurring in the conduit is studied in an integral way.

A practical measure of changes in peak concentration is looking at the ratio of two successive concentration amplitudes, in which amplitude is defined as the difference between the peak concentration $c_{v,p}$ and the trough concentration $c_{v,t}$. We take the natural logarithm of this ratio (known as the logarithmic decrement) as a measure indication of the overall attenuation of concentration gradients after a certain propagation distance, e.g. after full passage through the conduit (in which case i denotes the number of cycles) or between two CCM's (in which case i denotes the CCM index):

$$\delta = ln \frac{|c_{v,p} - c_{v,t}|_i}{|c_{v,p} - c_{v,t}|_{i+1}} \tag{15}$$

The logarithmic decrement δ will be used to compare the attenuation of concentration gradients for different types of sediments under different conditions. When relating δ to c_v, c_v is calculated as the average value between the successive measurement points as $\overline{c_v} = 1/2 \cdot \left(c_{v,i} + c_{v,i+1}\right)$.

4. Results and discussion

4.1. Overview of flow conditions

We have analyzed the experiments using the Equations described in Section 3.3. When the mixture velocity is required, we have taken the mean of the measured mixture velocity as the representative velocity, neglecting the start up of the conduit. The terminal settling velocity v_{ts} is based on Eq. (10) using the viscosity of fresh water at $T = 17\,°C$, while the particle response time t_p is based on solving the equation of motion of a submerged settling sphere (which, due to the lower drag coefficient compared to drag coefficient of sediment grain, will be on the lower end. The real response time could be slightly larger.). The axial dispersion coefficient ϵ_z is based on Taylor dispersion, which provides a measure of the total dispersion as if the particles would have zero inertia. We used $\tau_f/\rho_f = \lambda/8 \cdot v_m^2$ with $\lambda/8 \approx 0.1$ as a conservative estimate. decreasing effect of turbulent dispersion is expected with increasing St, and the relative importance of advection over turbulent dispersion also increases with increasing particle size (illustrated by the Pe number). An overview of results is presented in Table 2.

4.2. Fully dispersed results

We have followed the procedure of Clift and Manning-Clift [22] as presented in Section 3.3.1 to find the theoretical equilibrium concentrations in the riser and return pipe and to find the mixture wall shear stress. The results are shown in Figs. 5.

The delivered concentration c_{vd} correlates with the equilibrium concentration $c_{v,eq}$, within a bandwidth of +50% and −10%, so an upward bias is observed. Since the equilibrium concentration $c_{v,eq}$ is based on the actual mass of sediment inserted in the system, the bias should be explained as measurement inaccuracy.

The riser and return pipe concentrations as determined with the differential pressure measurements (Eqs. (5) to (13)) correlate with the concentrations as measured with the CCM's within a bandwidth of +100% and −25%, so again an upward bias for the measurement with the differential pressure sensors. The wall shear stress τ_m as a function of mixture velocity shows no clear correlation for the velocity range under investigation. The $d_m = 0.42$ mm data have more or less equal concentrations at the three data points ($0.04 < c_{v,eq} < 0.05$) and the wall shear stress is approximately 20 kPa at the three velocities. The other data points have a larger variation in concentrations, which explains the scatter in shear stress at equal velocities. This clearly shows when we plot the wall shear stress versus the delivered concentration. There is a distinct upward trend ranging from 11.46 Pa to 34.82 Pa which is in line with expectations. No clear relation between particle size and friction can be found from the data, which most probably is due to the relatively small concentrations and inherently small solids effect to the overall friction.

Given continuity throughout the conduit, we expect the concentrations in the riser to be larger than the concentrations in the return pipe, with an increasing difference with increasing particle size (due to the larger change in slip velocities, see Eq. (11)). The ratio $c_{v,r}/c_{v,rp}$ as measured using both the differential pressure sensors and CCM's are plotted versus $R = c_{v,r}/c_{v,rp}$ as calculated with Eq. (12), see Fig. 6. It shows that the ratio of concentrations as determined with the differential pressure sensors correlates well with the theoretical relationship and the ratio is consistently larger than 1, which is in line with expectations. Furthermore, we see an increasing ratio with increasing particle size, which is consistent with theory as well.

On the contrary, looking at the same comparison with the CCM data, we see also ratios smaller than 1, which is not realistic. The relation between particle size and R is also inconsistent. In the lower range of the CCM's, the combined inaccuracies of temperature effects and calibration seem to be influencing the analysis. The results could be improved by evaluation of the carrier fluid properties (temperature and conductivity) before and after each experiment. This would allow for correction of the data afterwards.

4.3. Transient results: attenuation of concentration gradients

Each experiment started with a loosely packed batch of sediments sitting on a closed gate valve at the position of CCM1. After starting the pump and opening the valve, the batch starts being fluidized by the developing upward flow of water. The fluidized batch will have a smaller concentration than the loose packing when it gets into motion and accelerates upward in the direction of CCM2. In the upward motion

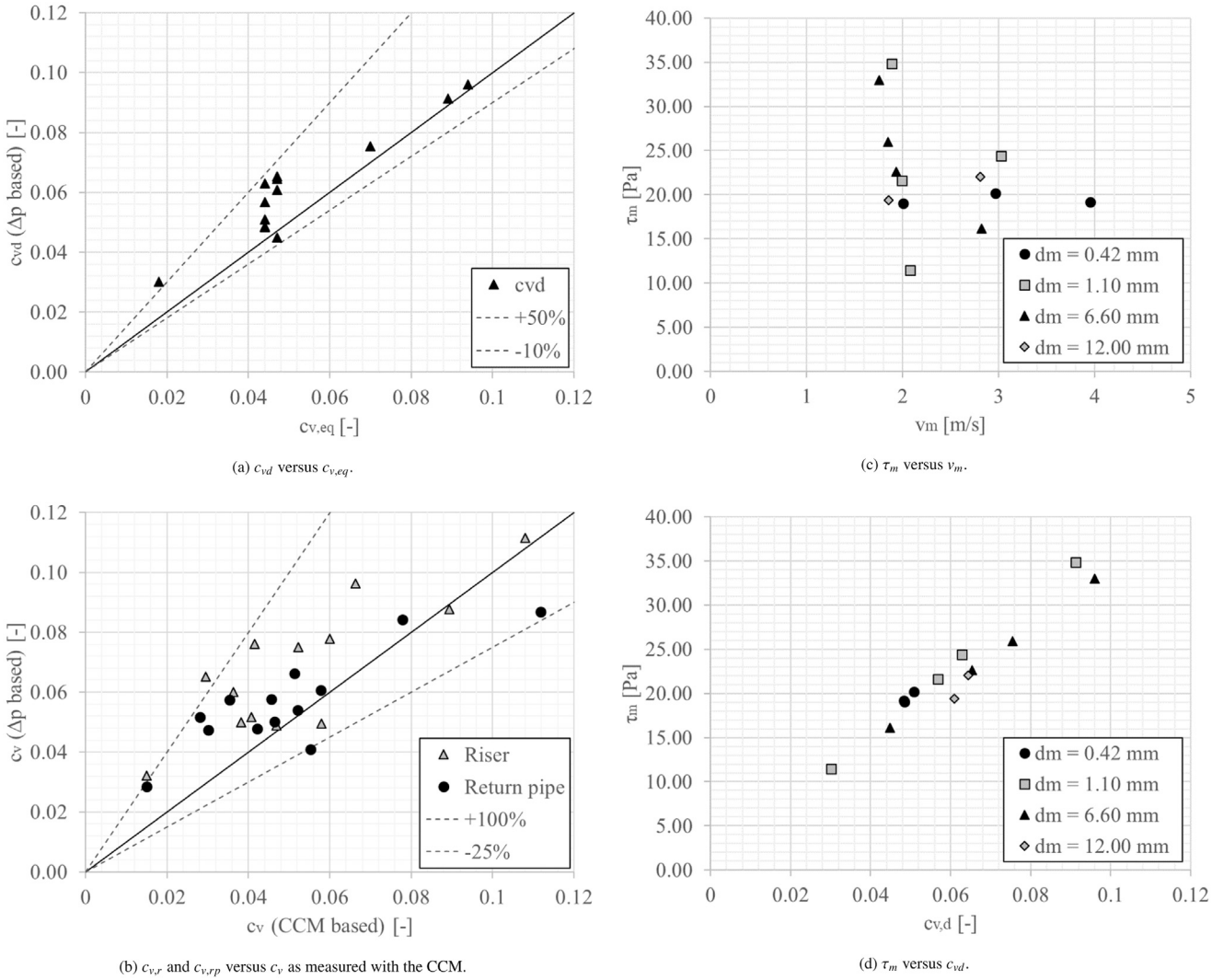

(a) c_{vd} versus $c_{v,eq}$.

(c) τ_m versus v_m.

(b) $c_{v,r}$ and $c_{v,rp}$ versus c_v as measured with the CCM.

(d) τ_m versus c_{vd}.

Fig. 5. Results of the quasi steady-state analysis show the correlation between the delivered concentration c_{vd} according to Clift and Manning-Clift [22] and the equilibrium concentration $c_{v,eq}$; the riser and return pipe concentrations $c_{v,r}$ and $c_{v,rp}$ as determined by Clift and Manning-Clift [22] and the CCM measurements; and the mixture wall shear stress τ_m shown versus the mixture velocity v_m and delivered concentration c_{vd}.

of the batch, hindered settling theory describes the solids velocity of the sediment particles in the batch.

When moving past CCM2, the batch will enter the horizontal top section of the pipe. In all experiments the mixture velocity is around 1–3 m/s, which is sufficiently low for the sand particles to show stratification (the concentration at the bottom of the horizontal pipe is larger than the concentration at the top of the horizontal pipe), while for the gravel particles a clear sliding bed develops. The propagation from CCM2 to CCM3 thus is governed by (highly) stratified or even sliding bed transport. To maintain a constant solids flux, the concentration of the batch will increase in this pipe section to compensate for the decreased solids velocity.

After leaving the horizontal top pipe, the batch passes CCM3 and further descends towards CCM4. Here the solids velocity is described again by hindered settling theory, but now with gravity being aligned with the flow direction rather than opposite, as was the case for the upward transport. As a result, the batch will dilute to account for the relatively high solids velocity.

The diluted batch will pass through CCM4 and will enter the horizontal pipe towards the centrifugal pump. Here, a complex interplay occurs between flow stratification, buffering and mixing in the pump. After leaving the pump, the batch will move upward again past CCM1. The entire passage through the circuit will eventually lead to dispersion of the solids and a decrease in peak concentration, but the effect of the individual sections on the total attenuation of the concentration gradients differs.

We have studied the attenuation (or growth) of the peak concentrations using the logarithmic decrement of Eq. (15). All data has been processed for 4 cycles through the conduit, and the minima and maxima in concentrations have been determined for every cycle. In the analysis we compare two pairs of CCM's to find a value of δ. In this way, we can look at the attenuation of the concentration over different parts of the conduit. For the riser, we have compared CCM1 and CCM2. For the return pipe, we have compared CCM3 and CCM4. For the top section, we have compared CCM2 and CCM3, and for the pump, we have compared CCM4 and CCM1. Each cycle of a sediment batch through the conduit thus gives four values of δ for the different sections in the conduit. We have combined the data of the four sections, for 4 cycles per experiment, in a single graph per sediment type. Experiment 11 has been discarded in the analysis because this experiment had an ill-conditioned startup phase, which made the batch transport too messy to analyze the first 4 cycles up to steady state conditions. The results are shown in Fig. 7.

The $d_m = 0.42$ mm results show an increase in δ with increasing peak concentration $c_{v,p}$ (largest concentration of the batch when it passes the CCM) for all sections of the conduit. We see the pump introduces the

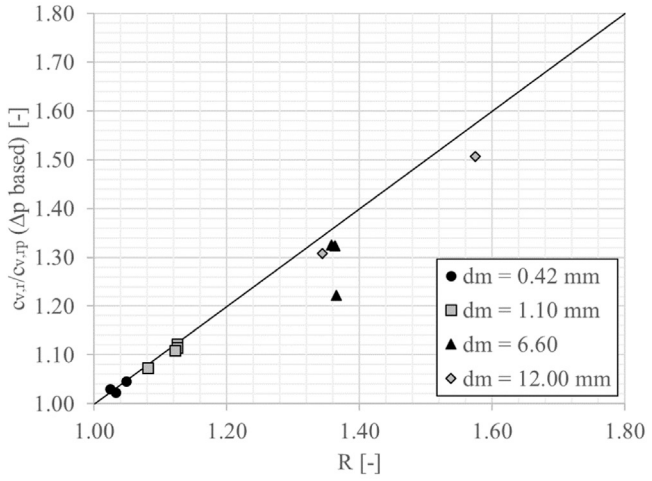

(a) $c_{v,r}/c_{v,rp}$ as measured with the differential pressure sensors versus R.

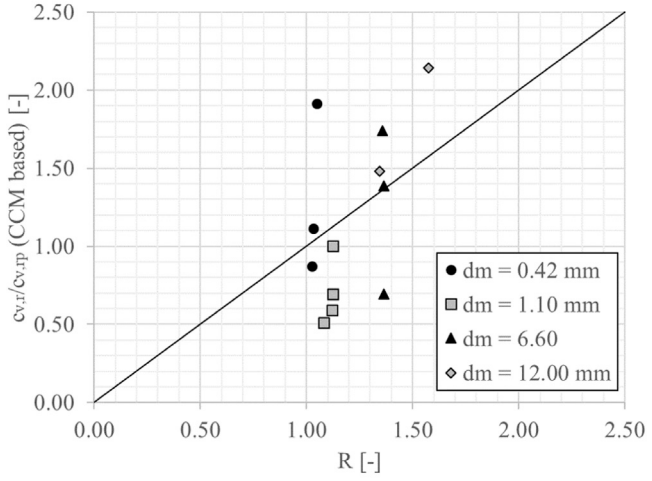

(b) $c_{v,r}/c_{v,rp}$ as measured with the CCM's versus R.

Fig. 6. The ratio $c_{v,r}/c_{v,rp}$ shows how the concentrations differ between the riser and return pipe in the conduit due to gravity and the resulting differences in slip velocity with flow direction. The differential pressure measurements show consistent results with theory, but the CCM data does not.

largest attenuation of the concentration peak with $\delta > 0.2$, while the top section even increases the concentration peak, which is shown by negative δ values. The riser sections shows $0 < \delta < 0.2$ for $c_{v,peak} < 0.2$, which is smaller than the attenuation found in the return pipe with $0 < \delta < 0.3$ for $c_{v,peak} < 0.2$. For larger concentrations, the δ's in the riser and return pipe are comparable.

The $d_m = 1.10$ mm results show the largest attenuation of the concentration peak at the pump, and it shows an even more pronounced increase in concentration peaks at the top section compared to the $d_m = 0.42$ mm data. There is no clear increase of δ with $c_{v,p}$, and the δ values for riser and return pipe are of similar magnitude with $0 < \delta < 0.4$ for $c_{v,peak} < 0.5$.

When we look at the $d_m = 6.60$ mm gravel, we see an interesting phenomenon: the pump now introduces negative δ's while the top section shows the largest δ values. The pump causes an increase in the peak concentration while the top section introduces the strongest attenuation, which is the complete opposite of what was observed for the sand. The riser and return pipe introduce attenuation of the concentration peak of the same magnitude. Values of $\delta \approx 0$ or even negative values are observed for the riser and return pipe, while for the sand there was clear attenuation.

The $d_m = 12.00$ mm gravel shows $\delta < 0$ or increase in concentration peak at the pump and at the top section, while the top section also shows large attenuation at similar concentrations. The δ values for the riser are small, with $\delta < 0.2$ or even negative, while the return pipe in this case shows very large values of δ or large attenuation of the concentration peak.

The δ values close to zero as found in the riser for the gravel measurements point at the absence of attenuation of concentration peaks, which is in line with a strongly reduced axial dispersion coefficient found for increasing Stokes numbers of particles as reported in Van Wijk et al. [26]. Turbulent dispersion of these sediments hardly play a role which is confirmed by the large Peclet numbers of the gravel experiments. The large attenuation of the concentration peaks found in the return pipe consequently cannot be attributed to turbulent dispersion, and the effect that is observed here could only relate to the nonlinear dependency of the particle transport velocity on the concentration, see Eq. (11). When the batch moves downward in the return pipe, multiple effects take place. The weight of the batch helps the pump in accelerating the entire mixture, while the batch also accelerates downward due to gravity on the particles. The change in solids velocity can be observed in the velocity measurements as a fluctuation of ±10% on the signal. Looking at the solids flux $c_v \cdot v_s = constant$ due to continuity, the increasing solids velocity during the descend of the batch should result in a reduction of the concentration in the batch. Using Eq. (11) for the gravel with $v_{ts} = 0.58$ m/s, a change from $v_m = 1.5$ m/s to $v_m = 1.8$ m/s (based on the velocity measurement of experiment 12) would result in a concentration decrease from $c_{v,rp} = 0.05$ to $c_{v,rp} = 0.038$ under the condition of constant solids flux. This effect alone would give rise to $\delta = \ln(0.05/0.038) = 0.27$ which is in the correct order of magnitude. Extensive modeling of the total system and sediment dynamics is beyond the scope of the current research, but it should be clear from above discussion that a comprehensive understanding of the different effects is essential for accurate modeling of transients in hydraulic transport systems.

Looking at the Stokes numbers St in Table 2, we see $Stk > 1$ for the gravel, which means the gravel's inertia is dominant over the changes in the main flow condition. This means acceleration and deceleration of the particles when moving up and down the conduit legs are dominant over the main water flow dynamics. Next, these coarse particles tend to settle in the horizontal parts of the conduit (top section and pump section). When flowing horizontally in a sliding bed, the net solids velocity is much smaller than the vertical (upward or downward) transport velocity in the riser and return pipe. The concentration in the horizontal parts thus increases, sediments start accumulating. This shows in the $d_m = 12.00$ mm experiments. In the top section, the gravel forms a sliding bed of solids, and a thin layer of particles is slowly sliding into the return pipe. Saltation of particles and erosion can take place as well. The large attenuation of the concentration peak in the horizontal top section is due to material accumulation: CCM3 measures a smaller quantity of sediments than CCM2, because the influx past CCM3 is governed by the slowly sliding bed.

In the pump and surrounding horizontal pipelines the gravel forms a sliding bed again, with a transport velocity significantly smaller than the downward hindered settling velocity as was present in the return pipe. The net effect is again accumulation, but now with a reverse effect on δ The batch accelerated downward from CCM3 to CCM4, and CCM4 measures low concentrations compared to the concentrations in the bottom horizontal section and pump. The sliding bed then moves upward in the riser with smaller solids velocity than the downward velocity in CCM4, so CCM1 measured a larger concentration compared to CCM4, which shows as negative values of δ over the pump.

The sand experiments with $Stk < 1$ show the opposite: attenuation of concentration peaks in the pump, growth of concentration peaks over the top section. Since the sand follows the major fluctuations in the flow ($Stk < 1$), the internal flow in the centrifugal pump works as a large mixer. The sand gets mixed in a relatively large volume of water in

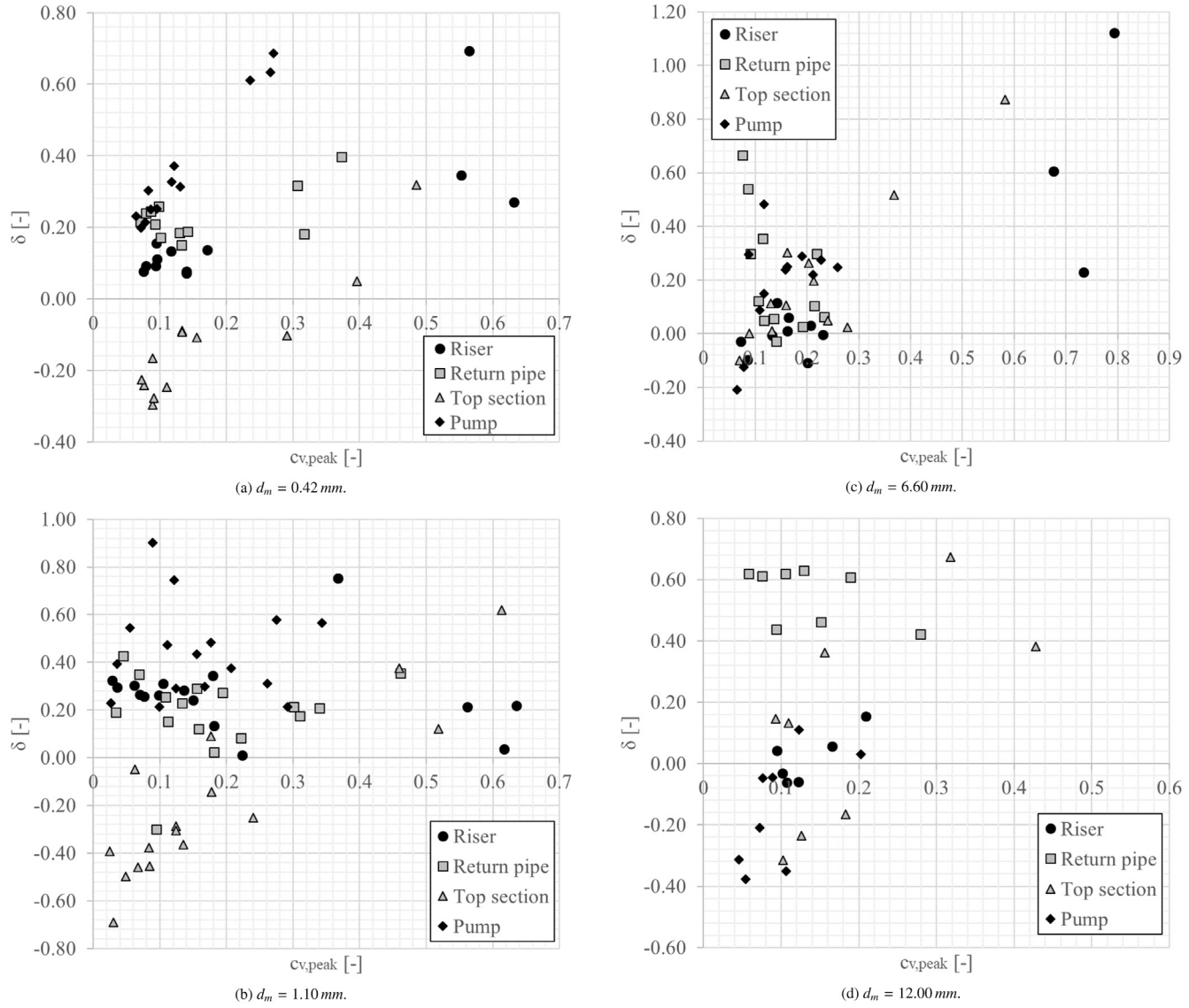

(a) $d_m = 0.42\,mm$. (c) $d_m = 6.60\,mm$.

(b) $d_m = 1.10\,mm$. (d) $d_m = 12.00\,mm$.

Fig. 7. Logarithmic decrement δ of Eq. (15) as found for the riser, return pipe, top section and pump for the different sediment types, analyzed for 4 cycles through the conduit. Experiment 11 has been discarded in this analysis.

the pump (locally) before it enters the riser section and CCM1, acting as a minor buffer to the mixture, which suppresses the concentration peaks. Since the flow stratification is much less for the sand than for the gravel, it is not the sliding bed or stratified flow that governs the total solids flux, but it is the mixed flow and buffer function of the pump. The mixture flowing past CCM1 thus shows a smaller concentration peak.

The remaining question is why the top section shows large negative values of δ in case of $Stk < 1$. Although no sliding bed occurs as is the case with gravel, the sand still accumulates in horizontal sections. In the bottom part we identified the pump as a buffer/mixer, which counteracts the stratification effect of the horizontal pipework. The net effect is a decrease in concentration of the solids passing CCM1 compared to CCM4. In the top section, the solids velocity in the horizontal part is smaller than the upward solids velocity, so accumulation occurs as well. In this case, the accumulation is not counteracted by the buffer/mixer effect of the pump, and it is the associated increase in concentration that governs the solids flux downward past CCM3. While for gravel the accumulation shows as a sliding bed, and the flux past CCM3 was governed by the sliding bed velocity, for the sand the increased concentration shows as a mildly stratified flow without a sliding bed. Consequently, CCM3 sees an increased concentration before attenuation during the downward free fall of the batch counteracts this effect again. Next to that, when a sliding bed of solids moves from the top horizontal section into the return pipe, a new flow regime is developing and the solids have an uneven distribution over the cross section. The CCM's sensitivity to spatial solids distributions over the cross section has not been investigated.

In summary, we see that local system effects play an important role in the overall system behavior, an effect that becomes more pronounced with increasing sediment size (and associated increase in Stokes number St).

5. Conclusions and recommendations

The CCM sensors are very sensitive to the water temperature. Single point temperature measurement as conducted in these experiments proved to be insufficient to accurately correct the CCM's readings due to the presence of an initial temperature gradient in the conduit. An alternative correction methodology was followed to correct the readings based on initial conditions and equilibrium (well mixed steady-state) conditions, which was, for each experiment, at the end of an experiment. For future work it is advised to equip each CCM sensor

with an individual fast responding temperature sensor and to refresh the water in the system before each new experiment. This will enhance the overall accuracy of the CCM's.

The conversion from conductivity measurements with the CCM to solids concentrations requires careful calibration. Earlier research has shown that in the current CCM configuration there is a dependency on particle size, especially when using particles in the millimeter scale and above. It is necessary to calibrate the CCM's for each new sediment type to ensure the best performance. Calibration was done so to match the equilibrium concentration as if all particles would be homogeneously dispersed throughout the system, and secondly the resulting initial concentration as measured with CCM1 (at the lowest elevation in the conduit) was checked with the packed bed concentration as based on the actual inserted mass. It proved that the initial concentration was determined within 25% accuracy except for one outlier. However, similar sediments did not give similar calibration parameters in all cases, an effect which cannot be attributed to the CCM configuration. Probably, temperature effects and the presence of conductive material have played a role as well. The high sensitivity to temperature and conductive soluble matter is a downside of the CCM application with natural sediments.

We analyzed the equilibrium conditions after the batch was completely dispersed in the conduit and we found that the solids transport velocity ratio (using hindered settling theory superposed on the mixture velocity) gives a good estimate of the ratio between the concentration in the riser and return pipe. We found consistent results with the concentration measurements based on the differential pressure sensors, showing an increasing difference in concentration between riser and return pipe with increasing particle size. However, when using the CCM's for the same purpose, we found these measurements to be insufficient and inconsistent. The CCM's were calibrated using the average of concentrations in the riser and return pipe, and probably the inaccuracy of this method masks the subtle concentration differences occurring in practice. Note the inherently weak link between the two pairs of CCM's in riser and return pipe, since these were matched on initial conditions of CCM2 and CCM3 respectively.

The mixture wall shear stresses found in the analysis show a consistent, approximately linear, upward trend with the solids concentration for velocities in the range $2 < v_m < 4$ m/s, while no clear correlation could be observed with mixture velocity. This could be partially explained by the relatively small range of velocities investigated in this research. Under the investigated conditions, the mixture wall shear stress shows a much stronger correlation to the delivered concentration than to the mixture velocity. No significant differences could be found between the different particle sizes.

Although the absolute concentrations measured with the CCM's only have limited accuracy, detailed analysis of the attenuation or growth of concentration peaks in the system was still possible. To this end we defined the logarithmic decrement which considers the ratio of maximum and minimum concentrations of a batch passing two successive CCM's. This relative measure is not influenced by the absolute accuracy of the CCM's, it is calibration-independent, and since all signals experience the same ambient conditions with equal influence on all CCM's, the relative measure is believed to be much more accurate than the absolute reading. The logarithmic decrement method is applicable to all types of concentration measurements.

The logarithmic decrement was used to analyze the system on component level, being the riser, return pipe, horizontal top section and the pump. For the measurements with sand, having Stokes numbers smaller than 1, we found attenuation of the concentration peaks in the riser, return pipe and pump. We found growth of concentration peaks in the horizontal top section.

The measurements with gravel, having Stokes numbers larger than 1, also showed attenuation of the concentration peaks in the riser and return pipe, however the effects for the horizontal top section and pump were the opposite of the sand measurement. For gravel, we found very strong attenuation of the concentration peak at the top horizontal section, while we found actual concentration peak growth over the pump section. This different behavior on component level is related to the change in flow regimes (vertical upward, downward and horizontal) and the associated change in solids transport velocity and thus local concentrations. The sediment flow regime in the horizontal sections is governing, which strongly relates to particle size, and is believed to explain the difference between the sand and gravel measurements.

The gravel measurements even showed minor growth in peak concentration in the riser section, while consistent attenuation was found for the return pipe. It is reasoned that, given the large Stokes numbers and Peclet numbers in the different gravel experiments ($d_m = 6.60$ mm and $d_m = 12.00$ mm), in these systems turbulent dispersion hardly plays a role and global system dynamics and the nonlinear relation between solids transport velocity and solids concentration are governing the overall system response.

The different flow regimes occurring with the different sediments and flow velocities could result in uneven solids distributions over the cross section of the CCM's, depending on their orientation. This has not been considered in the current research, but it is recommended to be considered in future work.

CRediT authorship contribution statement

J.M. van Wijk: Conceptualization, Methodology, Formal analysis, Investigation, Writing – original draft, Visualization. **E. de Hoog:** Validation, Investigation, Writing – review & editing. **A.M. Talmon:** Review. **C. van Rhee:** Review.

Declaration of competing interest

The authors declare that they have no known competing financial interests or personal relationships that could have appeared to influence the work reported in this paper.

Acknowledgments

The work presented in this article received funding from Royal IHC, The Netherlands. The authors wish to thank Pieter Smit and Thomas Fonville for their invaluable contribution to the experimental work.

References

[1] V. Matousek, M. Kesely, Z. Chara, Effect of pipe inclinination on internal structure of settling slurry flow at and close to deposition limit, Powder Technol. (343) (2019) 533–541.
[2] E. De Hoog, J.M. in 't Veld, J.M. Van Wijk, A.M. Talmon, An experimental study into flow assurance of coarse inclined slurries, in: 18th International Conference on Transport and Sedimentation of Solid Particles, Prague, Czech Republic, 2017, pp. 113–120.
[3] A.M. Talmon, L. Aanen, R. Bakker-Vos, Laboratory tests on self-excitation of concentration fluctuations in slurry pipelines, J. Hydraul. Res. 45 (5) (2007) 653–660.
[4] H.P. Rice, Transport and deposition behaviour model slurries in closed pipe flow, (Ph.D. thesis), University of Leeds, 2013.
[5] K.C. Wilson, G.R. Addie, A. Sellgren, R. Clift, Slurry Transport Using Centrifugal Pumps, third ed., Springer Science and Media, 2006.
[6] R.G. Gillies, Pipeline flow of coarse particle slurries, (Ph.D. thesis), University of Saskatchewan, 1993.
[7] J. Evans, C.A. Shook, Dispersion and slip effects in hydraulic hoisting of solids, Can. J. Chem. Eng. 69 (1991) 1166–1173.
[8] J.M. Van Wijk, Vertical hydraulic transport for deep sea mining, a study into flow assurance, (Ph.D. thesis), Delft University of Technology, 2016.
[9] T. Mueller, J.M. van Wijk, H. Mischo, EU blue mining project - building a large scale test system and flow tests for vertical transport systems in deep sea mining (original in german), Georesources J. 3 (2018) 38–45.
[10] E. De Hoog, A.M. Talmon, C. Van Rhee, Unstable transients affecting flow assurance during hydraulic transportation of granular two phase slurries, J. Hydraul. Eng. 9 (147–04021029) (2021) 1–12.
[11] G. Falcone, G.F. Hewitt, C. Alimonti, Multiphase Flow Metering - Principles and Applications, in: Elsevier Developments in Petroleum Science, Vol. 54, Elsevier, 2010.

[12] J.M. Van Wijk, B. Blok, The influence of grain size on the performance of conductivity concentration meters, Flow Measur. Instrument. 45 (2015) 384–390.
[13] T.C. Choy, Effective Medium Theory, Principles and Applications, in: International Series of Monographs on Physics, Vol. 102, Oxford Science Publications, 1999.
[14] J.A. Sorensen, G.E. Glass, Ion and temperature dependence of electrical conductance for natural waters, Anal. Chem. 59 (13) (1987) 1594–1597.
[15] S. Banisi, J.A. Finch, A.R. LaPlante, Electrical conductivity of dispersions: a review, Miner. Eng. 6 (4) (1993) 369–385.
[16] J.C.R. Turner, Two-phase conductivity: the electrical conductance of liquid-fluidized beds of spheres, Chem. Eng. Sci. 31 (1976) 487–492.
[17] H. Nasr-El-Din, C.A. Shook, J. Colwell, A conductivity probe for measuring local concentrations in slurry systems, Int. J. Multiphase Flow 13 (3) (1987) 365–378.
[18] P. Glasserman, D. Videla, U. Boehm, Liquid fluidization of particles in packed beds, Powder Technol. 79 (1994) 237–245.
[19] J. Xu, Y. Wu, Z. Zheng, M. Wang, B. Munir, H.I. Oluwadarey, H.I. Schlaberg, R.A. Williams, Measurement of solid slurry flow via correlation of electromagnetic flow meter, electrical resistance tomography and mechanistic modelling, J. Hydrodyn. 21 (4) (2009) 557–563.
[20] Y. Faraj, M. Wang, ERT investigation in horizontal and vertical counter-gravity slurry flow in pipelines, Procedia Eng. 42 (2012) 588–606.
[21] G.E. Archie, The electrical resistivity log as an aid in determining some reservoir characteristics, Petrol. Technol. (1422) (1942) 54–62.
[22] R. Clift, D.H. Manning-Clift, Continuous measurement of the density of flowing slurries, Int. J. Multiph. Flow. 7 (5) (1981) 555–561.
[23] J.F. Richardson, W.N. Zaki, Sedimentation and fluidisation: part I, Trans. Instn. Chem. Engrs. 32 (1954).
[24] P.N. Rowe, A convenient empirical equation for estimation of the Richardson and Zaki exponent, Chem. Eng. Sci. 42 (11) (1987) 2795–2796.
[25] R I Ferguson, M Church, A simple universal equation for grain settling velocity, J. Sediment. Res. 74 (6) (2004) 933–937.
[26] J.M. Van Wijk, C. Van Rhee, A.M. Talmon, Axial dispersion of suspended sediments in vertical upward pipe flow, Ocean Eng. 92 (2014) 20–30.
[27] J.M. Van Wijk, S. Haalboom, E. De Hoog, H. De Stigter, M.G. Smit, Impact fragmentation of polymetallic nodules under deep ocean pressure conditions, Miner. Eng. 134 (2019) 250–260.
[28] N. Cheng, Comparison of formulas for drag coefficient and settling velocity of spherical particles, Powder Technol. 189 (2009) 395–398.
[29] G.I. Taylor, Dispersion of soluble matter in solvent flowing slowly through a tube, Proc. R. Soc. A 219 (1137) (1953) 186–203.